FULL RESEARCH ARTICLE

Global local modeling of melt pool dynamics and bead formation in laser bed powder fusion additive manufacturing using a multi-physics thermo-fluid simulation

Faiyaz Ahsan[1] · Jafar Razmi[1] · Leila Ladani[1]

Abstract

Understanding the physical mechanism of laser–powder bed fusion (LPBF) additive manufacturing can benefit significantly through computational modeling. LPBF uses a laser heat source to melt a number of layer of powder particles and manufactures a part based on the CAD design. This work aims to assess the impact of Marangoni flow, buoyancy and recoil pressure to simulate the fluid flow around melt pool with a non-Gaussian laser beam to simulate the interaction between laser and powder bed. It was observed that velocity profile shows two peaks on either side of the highest temperature point owing to Marangoni convection on both sides due to gradient in surface tension. Dimensional analysis was also conducted based on Peclet number, Nusselt number and Marangoni number to determine the mode of heat transport at various laser power/scan speed combinations. Convective heat flow is the dominant form of heat transfer at higher energy input due to violent flow of the fluid and recoil pressure around the molten region, which can also create keyhole effect associated with defects such as porosities. The computational model was also validated by comparing solidified bead geometry with experimental data.

Keywords Metal additive manufacturing · Laser powder bed fusion · Thermo-fluid multiphysics modeling · Melt pool flow · Dimensional analysis

1 Introduction

Laser powder bed fusion (LPBF) is a type of additive manufacturing process that produces near net shape products by melting metallic powder using a laser heat source. Dimensional accuracy and surface roughness of the part largely depend on a number of parameters like laser power, beam diameter, powder particle size, laser scan speed, layer thickness, etc. due to repeated melting and cooling of solidified layers. These parameters can alter the heat transfer and fluid flow around the melt pool which in turn affect the final build [1–6, 37]. Achieving a defect-free component using this technique relies on understanding the core mechanism of how these process parameters affect the thermal and fluid behavior of the process. The melting and solidification over a small length of powder particles occur at an extremely short

period of time, making in situ analysis difficult. Temperature gradient and flow around the molten pool are closely related to each other which needs to be analyzed. This is why, significant computational modeling is conducted to understand the thermal transport and fluid flow phenomena in LPBF [7–15].

There are several boundary forces that need to be considered to construct an accurate multi-physics thermo-fluid model. Surface tension-driven Marangoni flow and recoil pressure are two of the most important forces to consider. Surface tension plays a significant role in melt pool where temperature gradient is prominent. For most of the materials, surface tension is low where temperature is high, and the value is high in lower temperature region. This variation in surface tension pulls the fluid from the center of the melt pool to the outer radius, termed as Marangoni flow, which is the tangential stress that acts on the melt pool due to the temperature gradient [16]. This force can induce both conductive and convective heat flux, but convection is the dominant form of mass transfer [17]. Velocity around the molten zone can vary from high to low temperature point depending on the intensity of the Marangoni flow. Surface tension also has the tendency to shrink the surface area, which can create

✉ Faiyaz Ahsan
  fahsan1@asu.edu

1 Ira A. Fulton Schools of Engineering, Tempe, AZ 85287, USA

balling effect that is detrimental to the quality of the final part. Recoil pressure is another aspect of the process that plays a crucial role at a high energy input when the temperature exceeds the evaporation point of the material. At this point, vaporization takes place, and a large amount of heat is taken away, minimizing the temperature and depressing the melt pool [18]. The high pressure combined with Marangoni force can create instability in the melt pool, which can form keyhole-sized bead containing defects such as porosities [19]. Buoyancy can have a significant impact as well in the melt pool. As the density of a material inversely varies with temperature, it pulls liquid back from the bottom of the melt pool to the top at the center owing to the temperature gradient [11]. Although surface tension forces are predominant in the melt pool, the role of density gradient should not be ignored.

The importance of fluid flow around melt pool and transport of heat due to the fluid motion can be conveniently analyzed using dimensionless numbers like Nusselt number, Peclet number and Marangoni number [20, 21]. Nusselt number and Peclet number indicate the heat and momentum transfer respectively, while Marangoni number is defined as ratio of Marangoni flow to heat diffusion rate. The relative transport of heat through convection and conduction in the process can be assessed using these numbers. These studies can pave the path to understand the inherent physics of powder bed fusion technique in a simplistic manner as a number of variables are combined. Dimensionless numbers can reduce the complications associated with a process significantly and analyze the effect of input variables using unitless parameters [3].

The values of thermo-physical properties like heat capacity, thermal conductivity and diffusivity of metallic powder are another aspect of LPBF process that needs to be accurately included in the computational modeling for the simulation to be accurate. These properties determine the rate at which heat is transferred to and from powder bed. So, the melt pool formation and microstructural properties of the final part rely on these properties. Most of the

computational models rely on numerical and analytical calculations to determine these properties [22, 23]. Due to the scarcity of available literature, these researchers tested some common metallic powders from room to elevated temperatures to find out the values of these temperature-dependent properties [24], which is expected to substantially improve the modeling efforts.

Although conduction heat transferred was considered to be the main transport of heat, [25] recent modeling efforts have showcased the fact that convection also plays a vital role in the melt pool [26, 27]. Despite the development of a lot of modeling and simulation in recent times, a comprehensive thermo-fluid modeling including experimentally obtained thermo-physical properties of powders is needed in literature. This work focuses to bridge this gap by developing a realistic multi-physics model of the process including the thermal effects, fluid dynamic in the melt pool and experimentally obtained thermo-physical properties. Temperature profile, melt pool velocity will be determined using energy, mass and moment equation. Model validation will be carried out by comparing the melt pool shape with experimentally obtained result for Inconel 718. Dimensional analysis plays an important role in thermo-fluid analysis. The impact of convective heat flow around the melt pool due to Marangoni convection, buoyancy force and recoil pressure will be assessed based on several dimensionless numbers like Marangoni number, Peclet number and Nusselt number which dictates the relative importance of convective heat transfer.

2 Modeling technique

2.1 Multiphysics model

Two models were built to conduct a comprehensive analysis of the process using COMSOL Multiphysics software that can smoothly combine the heat transfer and fluid flow physics. The first model was 3 dimensional (Fig. 1),

Fig. 1 **a** 3D Model setup, **b** 2D melt pool extracted from the 3D model
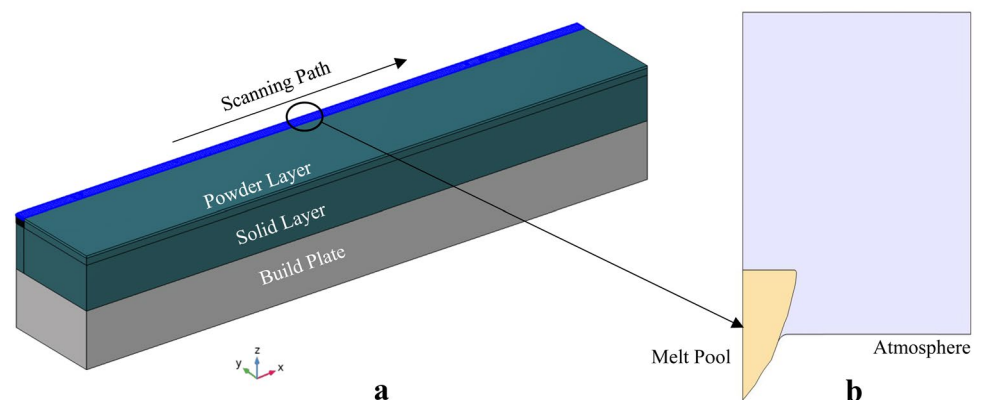
where the substrate was made of stainless steel, over which already solidified Inconel 718 is modeled. The powder bed surface is on top of that with a layer thickness of 0.04 mm. A moving laser heat source was modeled to interact with the powder bed using the following equation:

$$I(x,y,z) = \frac{2P}{\pi * w^2} * \exp\left[-\frac{2*(x^2+y^2)}{w^2}\right] * \exp(-\alpha * z)$$

$$\underset{\text{Radial}}{} \qquad \underset{\text{Along Depth}}{}$$

$$w = w_0 * \text{sqrt}\left[1 + \left(\frac{\lambda * z * M^2}{\pi * (w_0)^2}\right)^2\right]. \tag{2}$$

Here, P is the laser power, w_0 is the beam waist radius, λ is laser wavelength, M^2 is the beam quality factor, which indicates the variability of the beam from an ideal or Gaussian beam. The first term in Eq. 1 refers to the intensity of the laser beam in radial direction as the laser is scanned along the x axis. The 2nd term is the beer lambert law, which dictates heat distribution along depth. The 2nd model was built by extracting the region of the powder surface which was melted by the laser at a specific time, and atmosphere modeled using nitrogen. Level set method was used to get the solidified bead shape from melt pool that tracks the curve. The detailed description of the models can be found in our previous work [9].

2.2 Boundary conditions

The top surface of the model was exposed to radiation and natural convection with the atmosphere. Symmetry at y direction was used to save computational time [9].

The temperature gradient created during the process due to localized heating develop surface tension gradient on the powder bed surface. This gradient leads to Marangoni force, pulling fluid away from the hot region. This force acts as a normal component of the shear stress on the free surface of the fluid. This force is modeled with Navier–Stokes equation [28]:

$$\left[-pI + \mu(\nabla u + (\nabla u)^T - \frac{2}{3}\mu(\nabla.u)I)\right]n = \gamma \nabla_t T. \tag{3}$$

Here, p is the pressure, u is the velocity field, μ is the dynamic viscosity, γ is the Temperature derivative of surface tension.

Non-isothermal condition was applied in the whole domain where fluid properties like density, viscosity etc. are temperature-dependent [29]:

$$-n.q = \rho C_p^{\frac{1}{4}} k^{\frac{1}{2}} \frac{T_w - T}{T_{\text{amb}}}. \tag{4}$$

Here, q is the heat flux, ρ is the density, C_p is the heat capacity, T_w is initial surface temperature, T_{amb} is the ambient temperature and k is the thermal conductivity.

Recoil pressure was used on the surface only when the temperature exceeded the vaporization temperature of Inconel 718 which creates a depression in the melt pool [38]:

$$P_{\text{recoil}} = \frac{0.54 \times P}{1} \times \exp\left(\frac{H_v \times (T - T_{\text{ev}})}{R \times T \times T_{\text{ev}}}\right). \tag{5}$$

Here, H_v is the enthalpy of vaporization, T_{ev} is the vaporization temperature and R is the universal gas constant. The process parameters are listed in Table 1.

2.3 Material properties

To fill the gap of experimentally obtained data for thermophysical properties of Inconel 718, thermal diffusivity was measured using a DLF 1600 instrument up to 1400 °C, and heat capacity was measured using DSC 25 up to 625 °C. Thermal conductivity (Fig. 2) was calculated using the following equation:
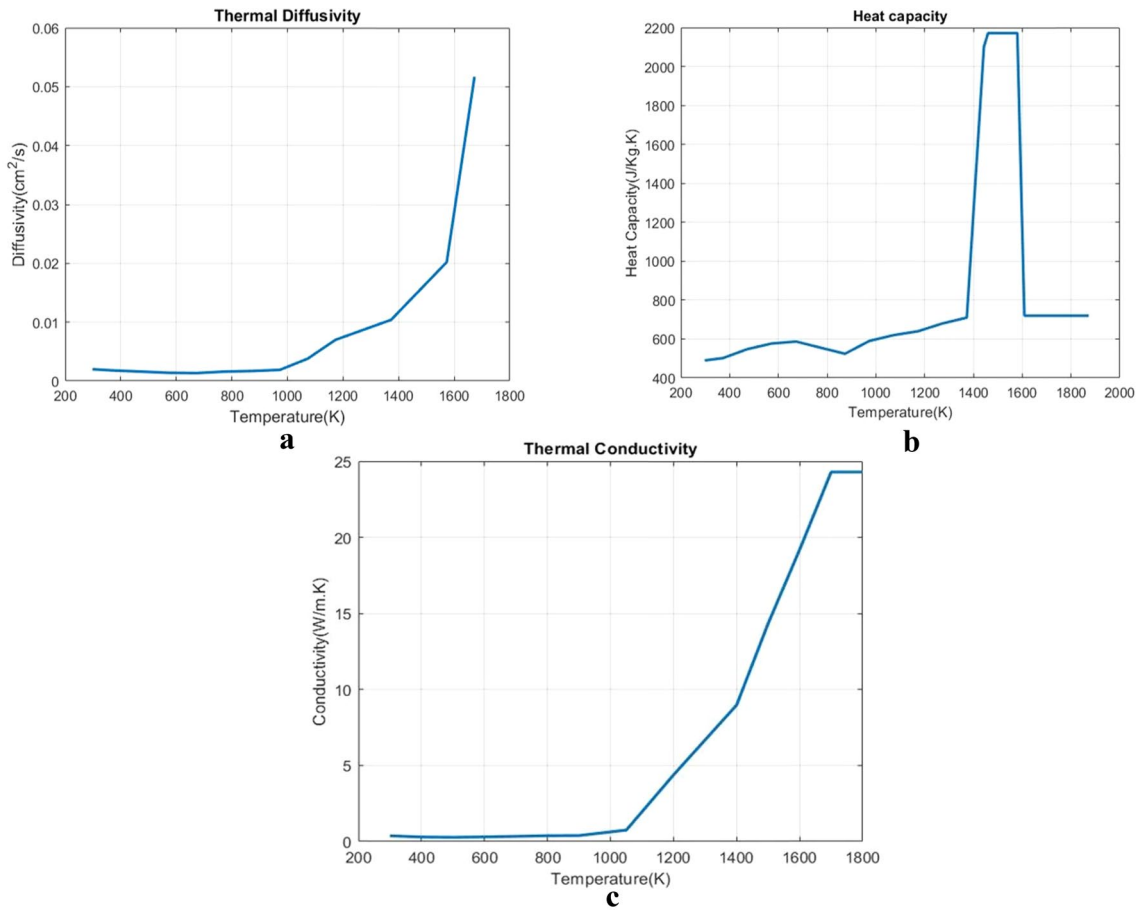
Thermal conductivity, $k = \alpha \times \rho \times C_p$. $\qquad$ (6)

Here α = Diffusivity, ρ = Density, C_p = Heat capacity

Diffusivity and conductivity values are low at lower temperature, but keeps increasing at elevated temperatures due to sintering of the powders, which increases the contact area. A detailed analysis of the experiments can be found in our previous work [24].

Other material properties like density, dynamic viscosity were imported from literature [39] (Fig. 3). These values decrease with increase temperature.

Table 1 Parameters used for simulation

Laser power (W)	100,150,200,300
Scanning speed (mm/s)	200,700
Layer thickness (mm)	0.04
Temp. derivative of surface tension (N/m K)	$3.7*10^{-4}$
Evaporation temperature (K)	3188
Enthalpy of vaporization (J/Kg)	$6.4*10^7$
Ambient temperature (K)	298
Laser spot diameter (um)	200

Fig. 2 **a** Thermal diffusivity, **b** Heat capacity, **c** Thermal conductivity of Inconel 718 measured experimentally at elevated temperature
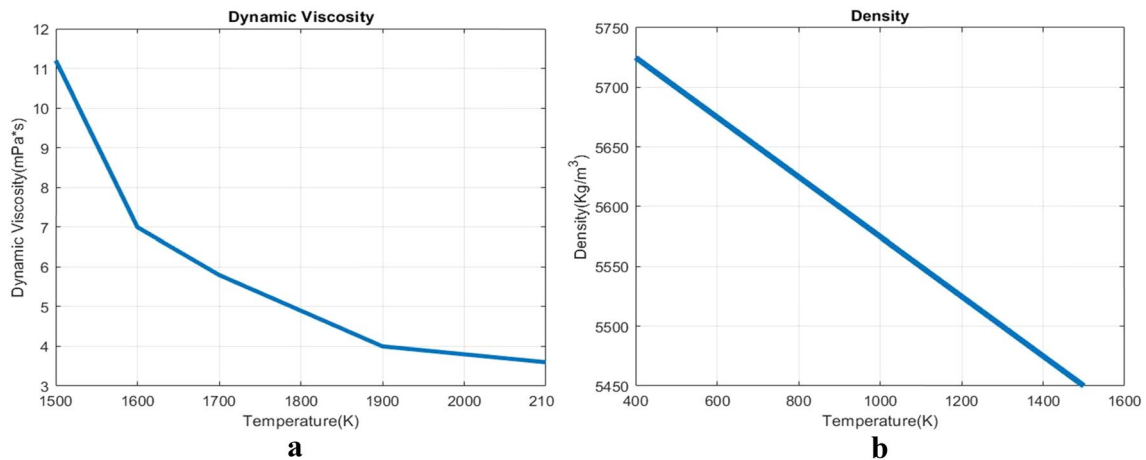
Fig. 3 **a** Dynamic viscosity, **b** Density of Inconel 718

2.4 Dimensionless numbers

In this paper, dimensional analysis was conducted to evaluate the effect of various mode of heat transport, such as conduction and convection, their relative importance in

the evaluation of molten pool and the parameters that can impact these processes.

Nusselt Number Nusselt number [30] is defined as a ratio between convective and conductive heat transfer. It provides a comparative analysis between the convective

and conductive flow. Nusselt number was calculated using the following process:

Internal Energy, $E = H - p/rho$

Convective Heat Flux, $Q_{conv} = \rho * u * E$

Convective heat transfer coefficient, $h = \frac{Q_{conv}}{T_{max} - T_s}$

$$Nusselt\ Number,\ Nu = \frac{h * l_{ch}}{k}. \tag{7}$$

Here, l_{ch}=Melt pool characteristic length, ρ= Density, H = Enthalpy, p = Absolute pressure.

Peclet Number Peclet number is the product of Reynolds and Prandtl number. Higher Peclet number signifies higher momentum transfer and flow rate as Reynolds No is a measure of flow rate and Prandtl no. It is the ratio of kinematic viscosity (measure of momentum transfer) to heat diffusivity (measure of heat transfer).

$$Peclet\ Number[31],\ Pe = Re * Pr = \frac{u * l_{ch}}{\alpha}. \tag{8}$$

Here, Re= Reynolds number, Pr= Prandtl number, l_{ch} =Characteristic length of the melt pool, u = velocity.

Marangoni Number Marangoni number (Ma) [32] is the ratio of surface tension-driven Marangoni force to viscous force within melt pool. Higher Marangoni number is an indication of convective heat transport in the fluid. Higher

Marangoni number can affect the dimension of the melt pool significantly.

$$Marangoni\ Number,\ Ma = -\gamma * l_{ch} * \frac{T_{max} - T_s}{\mu * \alpha}. \tag{9}$$

Here, T_s α= Solidus temperature of Inconel 718, = Thermal diffusivity

The dimensionless numbers are summarized in the following table (Table 2).

3 Results and discussion

This manuscript describes the overall heat transfer and fluid flow phenomena during powder bed fusion process based on various combination of laser power and scan speed. Result section is divided into various sub sections to clearly demonstrate different analysis.

3.1 Temperature profile

Temperature contour and profile along the scanning direction are shown in Fig. 4 at a specific time. Temperature is highest at the center of the beam owing to the maximum intensity at that point, then decays exponentially as it moves outward. As the beam has been modeled to follow a realistic pattern, it deviates slightly from an ideal or Gaussian beam. A comparison has also been drawn with our previous model [9]. The updated model has used experimental thermophysical properties at elevated temperature. We have also balanced the Marangoni force with Navier–Stokes equation, whereas the force was modeled as a weak expression in the previous model. This model includes recoil pressure as well that was missing from the previous one. As observed from

Table 2 Dimensionless Numbers

Dimensionless Number	Equation
Nusselt Number	$Nu = \frac{h * l_{ch}}{k}$
Peclet Number	$Pe = \frac{u * l_{ch}}{\alpha}$
Marangoni Number	$Ma = -\gamma * l_{ch} * \frac{T_{max} - T_s}{\mu * \alpha}$
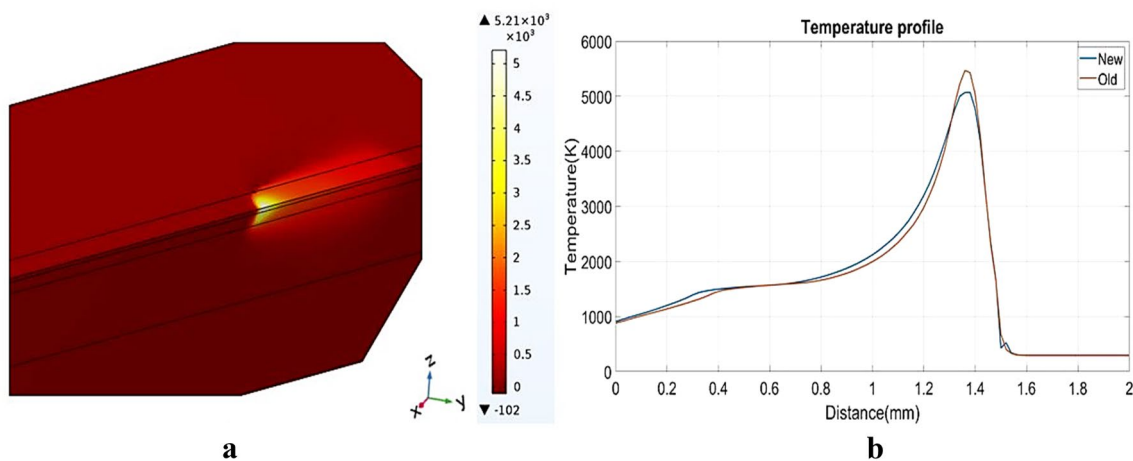
Fig. 4 **a** Temperature contour. **b** Temperature profile for new and old models at t = 0.0067 s for laser power = 300 W and scan speed = 200 mm/s

figure Fig. 4b, incorporating experimental material properties and recoil pressure has changed minimized the highest temperature by a margin of about 290 K. As the material temperature exceeds its vaporization temperature, the temperature decreases as energy is lost during vaporization process. The temperature profile has also turned wider as the gradient in surface tension has caused the liquid to flow from high to low temperature region and carry some heat with it.

3.2 Velocity profile

Figure 5a shows the fluid velocity contour at the $X–Y$ plane on the top surface at $z = 0$. At the center of the melt pool where temperature is maximum, velocity is low and increases toward both side of that point. This can be seen in Fig. 5b, where a plot is drawn along x axis, which is the scanning direction. There are 2 peaks on either side of the melt pool, among which the maximum velocity is achieved after the laser scanning point. This is due to the fact that surface tension forces are higher at high temperature gradient, propelling the fluid toward that direction at a higher speed. On the other hand, t peak has already been scanned, making that zone in a higher temperature region, making the flow of fluid lower. The same fact drives curve wider. The -y direction velocity is higher at the middle, along the radius of the melt pool. As we go further, the effect of surface tension diminishes, and no considerable velocity of fluid is visible.

3.3 Melt pool flow

Flow inside the melt pool is also shown Fig. 6 in along with the temperature contour to have a better understanding of the nature of the flow. The vector field is captured at a specific time. In Fig. 6c along the depth, there are two vortexes, one clockwise before the center of the beam, and one after the center of the beam having a counterclockwise direction. Around the top surface, the velocity is much higher because of the high surface tension gradient around the highest temperature region which is indicated by the thicker arrow lines. As we go deeper along the depth, velocity starts decreasing. Maximum velocity was found to 0.34 m/s, whereas minimum value was 0.11 m/s around the melt pool. Larger velocity indicates high convection heat transfer along the radius of the beam. Buoyancy also affects the melt pool. As the temperature is lower beneath the surface, the density of the material increases, which pushes the fluid upwards to the center of the molten pool. The effect of buoyancy is less nonetheless as observed from the thin vector fields compared to the. From Fig. 6b, direction of Marangoni flow is evident on the top surface. Fluid streams from the center to the edge of the laser beam, thus forming a melt pool. A cross section of the YZ plane (Fig. 6b) shows how the development of velocity helps to create a melt pool when the laser scans a particular point at a specific time under surface tension and gravity.
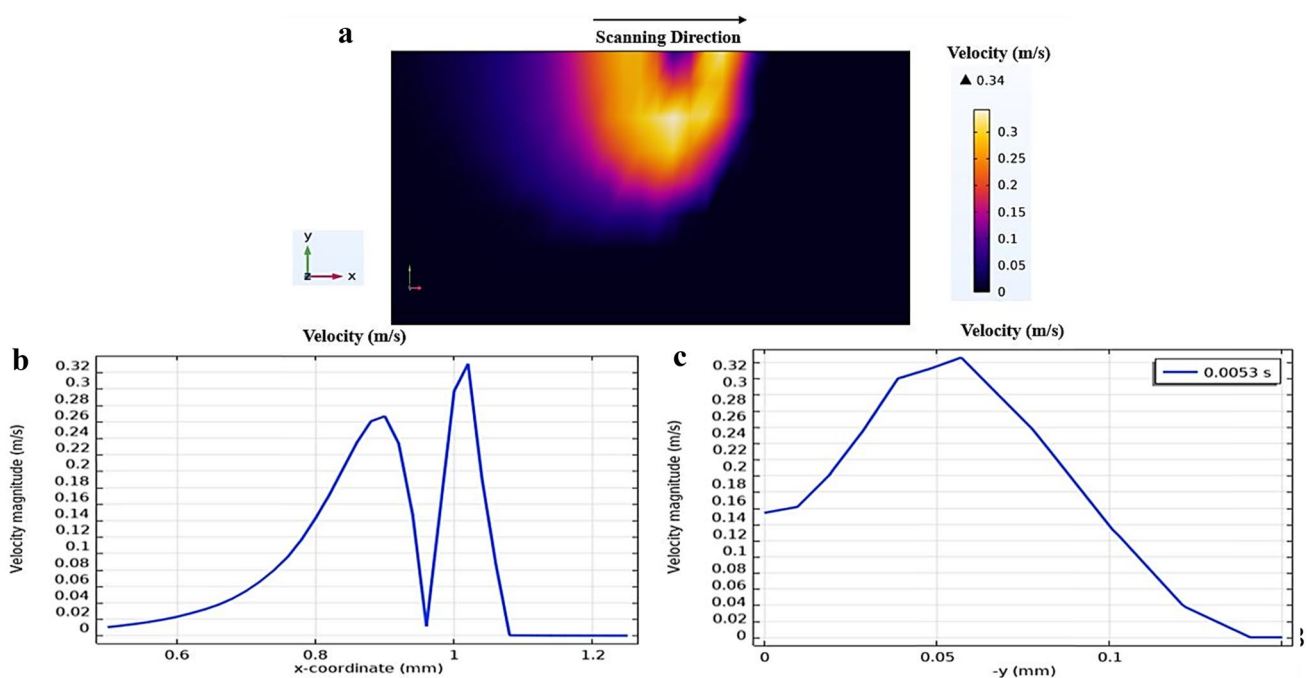
Fig. 5 **a** Velocity contour at the top surface. **b** Velocity profile at the scanning direction (x axis). **c** Velocity profile along -y direction for laser power = 300 W and scan speed = 200 mm/s
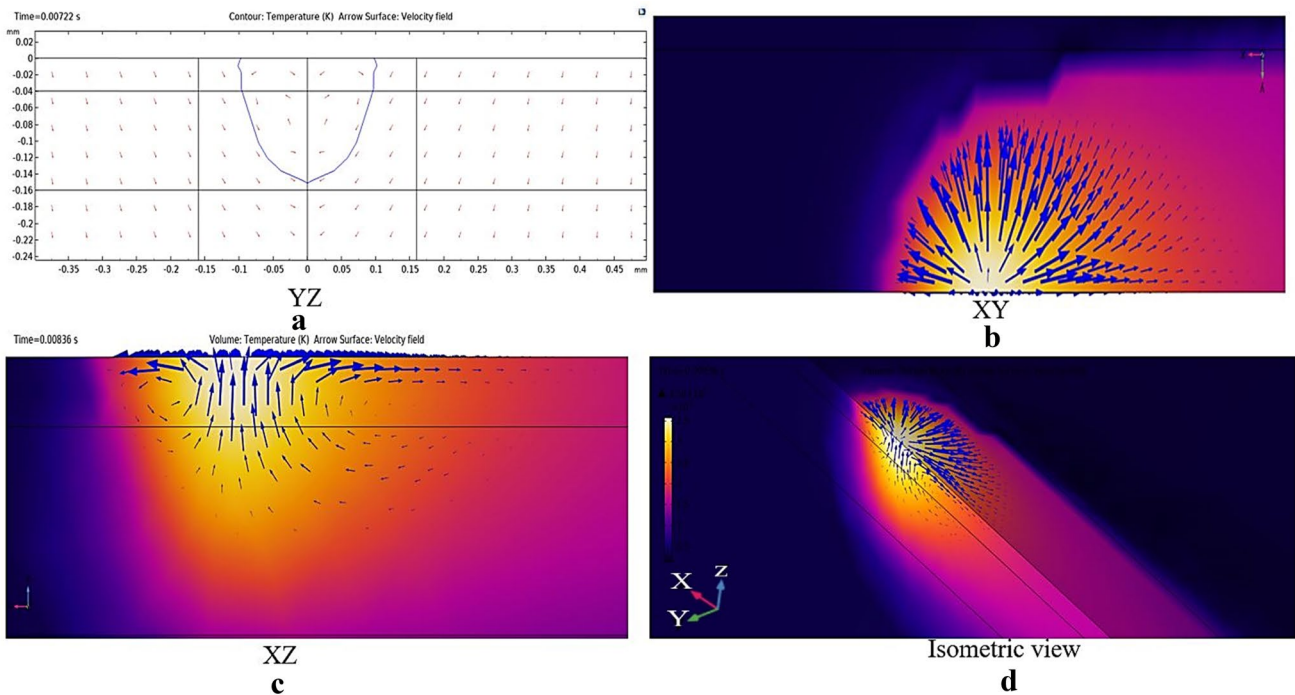
Fig. 6 Fluid flow arrow lines with temperature contour **a** *YZ* plane, **b** *XY* Plane, **c** *XZ* Plane, **d** Isometric view

3.4 Model validation

Experimental result from Sadowski et al. [33] from our group was used to compare the updated model against the previous one. For various laser powers ranging from 100 to 300 W at a scan speed of 200 mm/s, the results for melt pool width and depth are showed in Fig. 7. As expected, both width and depth increase significantly with higher power because of the greater energy input. Updated Marangoni force has improved the melt pool width significantly with the result being close to experimental values. Using recoil pressure to depress the melt pool at higher laser powers has also proved to be useful as the simulation result follow the experimental trend well. Melt pool depth was significantly higher than the layer thickness for higher power, indicating laser could penetrate through the substrate for initial layers.

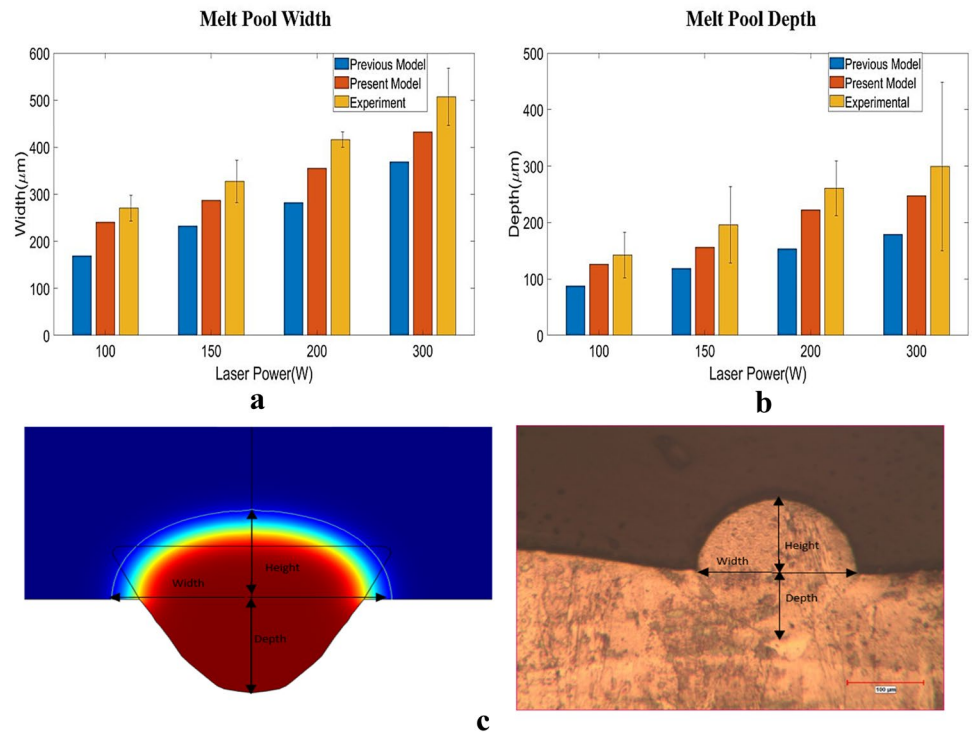The percentage error between experimental and numerical result is provided in Table 3

3.5 Dimensional analysis

Figure 8a shows the variation of Nusselt number along the laser scanning direction at a specific time for $300 \text{ W}/200 \text{mms}^{-1}$ combination. Nusselt number is low initially and start getting high when the powders get heated. Nu has two peaks and highest just after the scanning point, suggesting it is mainly driven by the convective flow of fluid within the melt pool. Figure 8b demonstrates the Peclet

number which shows similar pattern as the Nusselt number. Higher Peclet number indicates that momentum transfer is the more prominent feature compared to diffusion. Inconel 718 has a relatively lower thermal diffusivity, resulting in higher Peclet number.

Figure 9 represents the variation of Nusselt and Peclet number as a function of Marangoni number which is increasing with laser power input. As the Marangoni number increases, both Peclet and Nusselt number increase and significant amount of heat is transferred by convection. At smaller Pe and Nu numbers, convection is not significant, and conduction is the more dominant form of heat transport. As the Marangoni number increases, the fluid within the melt pool becomes more violent with increasing velocity, which induces convection. Peclet and Nusselt number higher than 20 [3] indicates that the momentum due to fluid velocity get increasingly dominant, which can even create pores and other defects within the melt pool that can be observed from experimentally obtained bead geometry. Generation of recoil pressure due to high process temperature along with larger melt pool area can depress the surface that can create keyhole along z axis of the melt pool [34]. The fluctuation in the met pool due to keyhole formation can trap the metal vapor within the keyholes that can create defects like porosities [35]. Figure 9 links high values of Peclet and Nusselt number that leads to such defects at higher energy input (Process parameters of 300 W/200 mm/s). The keyhole dynamics is a complex phenomenon which can arise due

Fig. 7 a Melt pool width. **b** Melt pool depth comparison against previous simulation and experimental results, **c** comparison of numerical and experimental bead shape

**Table 3** Percentage error between experimental and numerical result

Laser power (W)	Melt pool width (%)	Melt pool depth (%)
100	10.71	3.33
150	7.81	15.3
200	12.51	8.69
300	13.54	10.34

to a number of reasons. High Peclet and Nusselt number indicate instability in the melt pool which is one of the most dominant mechanisms behind this phenomenon. This can be better explained by constructing a turbulence model.

4 Discussion

This work was carried out to capture the multi-physics nature consisting of simultaneous heat transfer and fluid dynamic during the process (LPBF). An updated model based on our previous work was built including experimentally obtained thermo-physical properties at elevated temperatures, laser intensity profile along the depth that follows beer lambert law, Marangoni force, recoil pressure and buoyancy effect. Thermal response was captured first using energy, mass and momentum balance equation. Temperature profile is not symmetric because of the non-linear and non-Gaussian nature of laser–powder bed interaction during the process. Velocity of fluid reaches its peak immediately after the center

Fig. 8 a Nusselt number and **b** Peclet number as a function of position for 300 W/200 mm/s
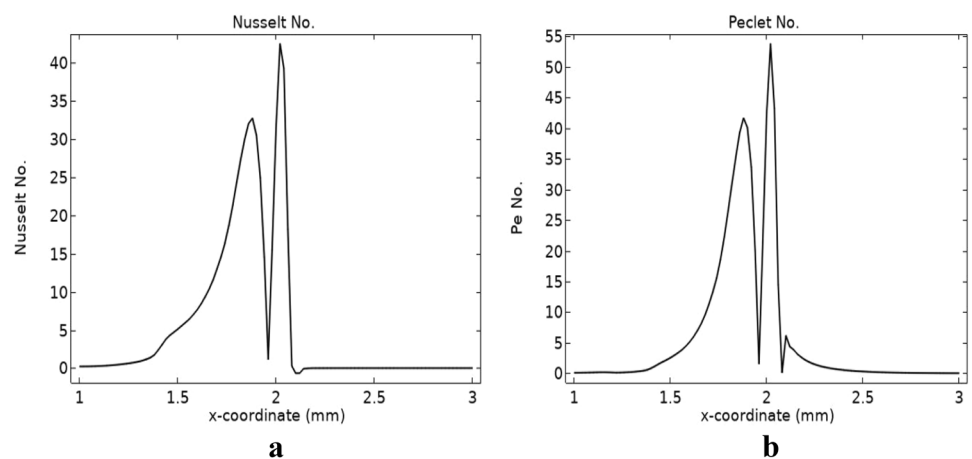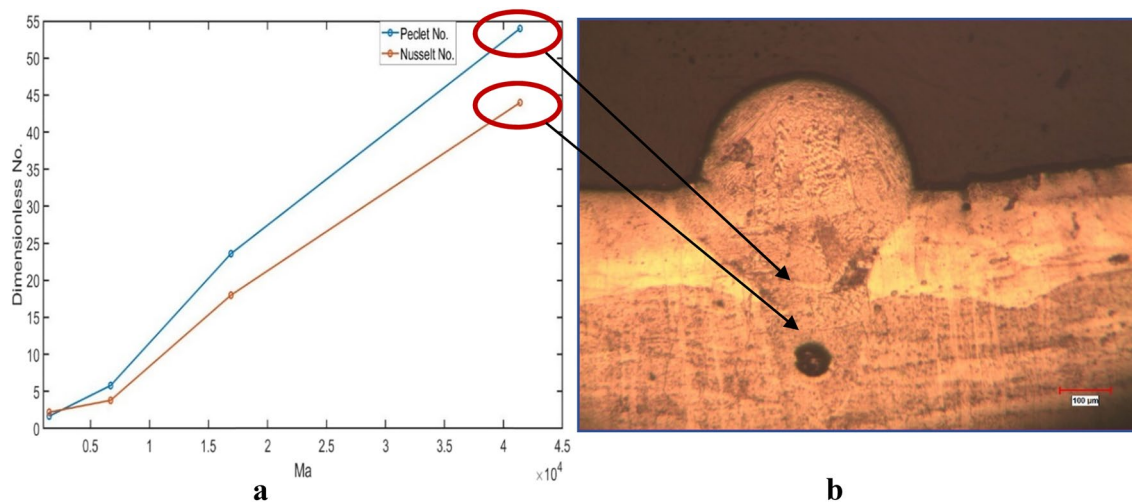
Fig. 9 **a** Peclet and Nusselt Number with increasing Marangoni Number for increasing laser power **b** Keyhole observed in the bead [33] at laser power and speed of 300 W/200 mm/s corresponding to Pe = 54, Nu = 44 and Ma = 41,000

of the beam due to higher thermal gradient around that region, prompting the fluid to accelerate toward the lower temperature point. The region before the highest temperature has a greater surface molten pool area as the laser has already scanned over that portion and temperature gradient is comparatively lower. The thermo-fluid model was able to perfectly capture the melt pool flow due to various driving forces. Fluid flows radially outwards due to the surface tension gradients and buoyancy drives the flow in the upward direction just below the center of the beam. The radial flow transfers heat from the center region to the molten pool, elongating both the length (*x* axis) and width (*y* axis) of the melt pool region [36]. Increase in laser power generally accompanies a gradual shift from conduction to keyhole type because of evaporation. Temperature exceeding the vaporization point creates recoil pressure, minimizing the highest temperature and creating a depression in the melt pool, which increases the depth of the molten region. Higher laser power generates significantly increased velocity, resulting in higher values of the dimensionless numbers like Nusselt number, Peclet number and Marangoni number. These dimensionless numbers are low at lower laser powers like 100 W, indicating heat is transferred away mainly through conduction from the hot region. Consequently, the melt pool size is small as there is not enough fluid movement to make a larger liquid zone that can create delamination due to lack of adhesion with the solid layer. As the power increases, melt pool starts to behave violently, making a possible transition from laminar to turbulent flow. Temperature difference inside the melt pool is low at higher Marangoni number, which minimizes the contribution from thermal conduction, and most of the heat is carried out by convection. This is evident from experimental image from Fig. 9, where the Peclet and Nusselt number are 54 and 44

respectively. The solid layers beneath the powder layer go through repeated melting and solidification because of deep melt pool, which can generate considerable residual stress in those layers. The image shows a keyhole formation that incorporates pores and other defects, indicating the intense nature of the fluid motion.

5 Conclusion

A robust three-dimensional thermo-fluid multi-physics model along with a 2-D model was built to analyze the thermal response and fluid flow of Inconel 718 during LPBF process. The major findings are summarized below:

- The temperature profile is lower and wider for the new model compared to the previous one owing to the updated material properties, surface tension properties and recoil pressure.
- Fluid flows on both sides of the center of the melt pool because of the high temperature gradient. The velocity is higher at the leading font of the melt pool.
- Melt pool expands in both *x* and *y* direction mainly due to violent Marangoni convection inside the melt pool. Melt pool depth depends on Marangoni convection, buoyancy, and recoil pressure.
- Both melt pool width and depth were validated against experimentally obtained data and improved results were observed.
- Contribution of convective heat transfer was established based on dimensionless numbers like Peclet, Nusselt and Marangoni numbers. At higher power, these numbers sig-

nificantly increase suggesting significant melt pool flow and subsequent convection.

References

1. Ali U, Fayazfar H, Ahmed F, Toyserkani E (2020) Internal surface roughness enhancement of parts made by laser powder-bed fusion additive manufacturing. Vacuum 177:109314. https://doi.org/10.1016/j.vacuum.2020.109314

2. Calignano F, Manfredi D, Ambrosio EP, Iuliano L, Fino P (2013) Influence of process parameters on surface roughness of aluminum parts produced by DMLS. Int J Adv Manuf Technol 67(9–12):2743–2751. https://doi.org/10.1007/s00170-012-4688-9

3. Mukherjee T, Manvatkar V, De A, DebRoy T (2017) Dimensionless numbers in additive manufacturing. J Appl Phys. https://doi.org/10.1063/1.4976006

4. Rahman MS, Schilling PJ, Herrington PD, Chakravarty UK (2019) Thermofluid properties of Ti-6Al-4V melt pool in powder-bed electron beam additive manufacturing. J Eng Mater Technol Trans ASME 141(4):1–12. https://doi.org/10.1115/1.4043342

5. Masoomi M, Soltani-Tehrani A, Shamsaei N, Thompson SM (2020) Convection heat transfer coefficients for laser powder bed fusion. In: Solid Free. Fabr. 2018 Proc. 29th Annu. Int. Solid Free. Fabr. Symp. - An Addit. Manuf. Conf. SFF 2018, pp. 1686–1693

6. Sing SL, Yeong WY (2020) Laser powder bed fusion for metal additive manufacturing: perspectives on recent developments. Virtual Phys Prototyp 15(3):359–370. https://doi.org/10.1080/17452759.2020.1779999 (**Taylor and Francis Ltd**)

7. Mian MJ, Razmi J, Ladani L (2021) Defect analysis and fatigue strength prediction of as-built Ti6Al4V parts, produced using electron beam melting (EBM) AM technology. Materialia 16:101041. https://doi.org/10.1016/j.mtla.2021.101041

8. Jafari D et al (2020) Pulsed mode selective laser melting of porous structures: structural and thermophysical characterization. Addit Manuf 35:101263. https://doi.org/10.1016/j.addma.2020.101263

9. Ahsan F, Ladani L (2020) Temperature profile, bead geometry, and elemental evaporation in laser powder bed fusion additive manufacturing process. Jom 72(1):429–439. https://doi.org/10.1007/s11837-019-03872-3

10. Rahman MS, Schilling PJ, Herrington PD, Chakravarty UK (2018) A comparative study between selective laser melting and electron beam additive manufacturing based on thermal modeling. ASME Int Mech Eng Congr Expo Proc. https://doi.org/10.1115/IMECE2018-86428

11. Ladani L, Romano J, Brindley W, Burlatsky S (2017) Effective liquid conductivity for improved simulation of thermal transport in laser beam melting powder bed technology. Addit Manuf 14:13–23. https://doi.org/10.1016/j.addma.2016.12.004

12. Ladani L, Ahsan F (2019) Laser interaction with surface in powder bed melting process and its impact on temperature profile, bead and melt pool geometry. Miner Metals Mater Ser. https://doi.org/10.1007/978-3-030-05861-6_29

13. Li X, Zhao C, Sun T, Tan W (2020) Revealing transient powder-gas interaction in laser powder bed fusion process through multiphysics modeling and high-speed synchrotron x-ray imaging. Addit Manuf 35:101362. https://doi.org/10.1016/j.addma.2020.101362

14. Rahman MS, Schilling PJ, Herrington PD, Chakravarty UK (2020) Heat Transfer and Melt-Pool Evolution During Powder-Bed Fusion of Ti-6Al-4V Parts Under Various Laser Irradiation Conditions. https://doi.org/10.1115/imece2020-23838

15. Bikas H, Stavropoulos P, Chryssolouris G (2016) Additive manufacturing methods and modeling approaches: a critical review. Int J Adv Manuf Technol 83(1–4):389–405. https://doi.org/10.1007/s00170-015-7576-2

16. Shen H, Yan J, Niu X (2020) Thermo-fluid-dynamic modeling of the melt pool during selective laser melting for AZ91D magnesium alloy. Materials (Basel) 13(18):1–19. https://doi.org/10.3390/ma13184157

17. Zhang D, Zhang P, Liu Z, Feng Z, Wang C, Guo Y (2018) Thermofluid field of molten pool and its effects during selective laser melting (SLM) of Inconel 718 alloy. Addit Manuf 21:567–578. https://doi.org/10.1016/j.addma.2018.03.031

18. Bayat M, Nadimpalli VK, Mohanty S, Hattel JH (2020) Resolving the effects of local convective heat transfer via adjustment of thermo-physical properties in pure heat conduction simulation of Laser Powder Bed Fusion (L-PBF). In: IOP Conf. Ser. Mater. Sci. Eng., vol. 861, no. 1. https://doi.org/10.1088/1757-899X/861/1/012006

19. Chen Y et al (2020) In-situ Synchrotron imaging of keyhole mode multi-layer laser powder bed fusion additive manufacturing. Appl Mater Today 20:100650. https://doi.org/10.1016/j.apmt.2020.100650

20. Wang Z, Liu M (2019) Dimensionless analysis on selective laser melting to predict porosity and track morphology. J Mater Process Technol 273:116238. https://doi.org/10.1016/j.jmatprotec.2019.05.019

21. Rankouhi B, Agrawal AK, Pfefferkorn FE, Thoma DJ (2021) A dimensionless number for predicting universal processing parameter boundaries in metal powder bed additive manufacturing. Manuf Lett 27:13–17. https://doi.org/10.1016/j.mfglet.2020.12.002

22. Asakuma Y, Honda I, Yamamoto T (2019) Numerical approach to predicting the effective thermal conductivity of a packed bed of binary particles. Powder Technol 354:886–892. https://doi.org/10.1016/j.powtec.2019.07.023

23. Measurement and Prediction of the Thermal Conductivity of Powders at High Temperatures. https://repositories.lib.utexas.edu/handle/2152/68665. Accessed 29 Mar 29 2021

24. Ahsan F, Razmi J, Ladani L (2020) Experimental measurement of thermal diffusivity, conductivity and specific heat capacity of metallic powders at room and high temperatures. Powder Technol 374:648–657. https://doi.org/10.1016/j.powtec.2020.07.043

25. Foroozmehr A, Badrossamay M, Foroozmehr E, Golabi S (2016) Finite element simulation of selective laser melting process considering optical penetration depth of laser in powder bed. Mater Des 89:255–263. https://doi.org/10.1016/j.matdes.2015.10.002

26. Rauniyar SK, Chou K (2019) Melt pool analysis and mesoscale simulation of laser powder bed fusion process (L-PBF) with Ti-6Al-4V powder particles. JOM 71(3):938–945. https://doi.org/10.1007/s11837-018-3208-2

27. Zhang Y, Zhang J (2019) Modeling of solidification microstructure evolution in laser powder bed fusion fabricated 316L stainless steel using combined computational fluid dynamics and cellular automata. Addit Manuf 28:750–765. https://doi.org/10.1016/j.addma.2019.06.024

28. "What Is the Marangoni Effect?" https://www.comsol.com/multiphysics/marangoni-effect. Accessed 03 Mar 2021

29. "Nonisothermal Flow." https://www.comsol.com/multiphysics/nonisothermal-flow. Accessed 03 Mar 2021

30. Roy U, Roy PK (2020) Advances in heat intensification techniques in shell and tube heat exchanger. In: Advanced Analytic and Control Techniques for Thermal Systems with Heat Exchangers, Elsevier, pp 197–207

31. Bender E (1981) Numerical heat transfer and fluid flow. VonS. V. Patankar. Hemisphere Publishing Corporation, Washington - New York - London. McGraw Hill Book Company, New York 1980. 1.

Aufl., 197 S., 76 Abb., geb., DM 71,90," Chemie Ing. Tech., vol. 53, no. 3, pp. 225–225. https://doi.org/10.1002/cite.330530323.

32. "Estimation of Marangoni number." https://pirika.com/ENG/ChemEng/Marangoni.html. Accessed 26 Mar 2021

33. Sadowski M, Ladani L, Brindley W, Romano J (2016) Optimizing quality of additively manufactured Inconel 718 using powder bed laser melting process. Addit Manuf 11:60–70. https://doi.org/10.1016/j.addma.2016.03.006

34. Lee JY, Ko SH, Farson DF, Yoo CD (2002) Mechanism of keyhole formation and stability in stationary laser welding. J Phys D Appl Phys 35(13):1570–1576. https://doi.org/10.1088/0022-3727/35/13/320

35. Repper E (2017) Defect formation in laser welded steels after use of corrosion protection coating

36. Shen H, Yan J, Niu X (2020) Thermo-fluid-dynamic modeling of the melt pool during selective laser melting for AZ91D magnesium alloy. Materials (Basel) 13(18):4157. https://doi.org/10.3390/ma13184157

37. Wang D, Linqing L, Guowei D, Cheng D, Yuchao B, Yongqiang Y, Weihui W et al (2022) Recent progress on additive manufacturing of multi-material structures with laser powder bed fusion. Virtual Phys Prototyp 1–37

38. Khairallah SA, Anderson AT, Rubenchik A, King WE (2016) Laser powder-bed fusion additive manufacturing: physics of complex melt flow and formation mechanisms of pores, spatter, and denudation zones. Acta Mater 108:36–45

39. Mills KC (2022) Recommended values of thermophysical properties for selected commercial alloys. Woodhead Publishing